Hydrogeology Journal (2022) 30:1637–1655
https://doi.org/10.1007/s10040-022-02504-6

PAPER

Controls on recharge in thick vadose zones under climate variability and change

Cassandra Wolf[1] · Jason J. Gurdak[1] · Zachary Lauffenburger[2] · Leora Nanus[3] · Ed Maurer[4]

Received: 5 January 2021 / Accepted: 7 June 2022 / Published online: 16 July 2022

Abstract

An improved understanding of recharge mechanisms and rates in relatively thick (14–38 m) vadose zones under irrigated and rangeland land use/land cover (LULC), climate variability, and future climate change can help inform sustainable groundwater management. Vadose-zone monitoring data from the High Plains aquifer in central USA were used to calibrate Hydrus-1D models and simulate recharge and total potential profiles during historical (1950–2018) and future (1950–2100) periods using an ensemble of nine downscaled global climate models (GCMs) at representative concentration pathways (RCPs) 4.5 and 8.5. Results show that historical recharge lag correlates with the Palmer Drought Severity Index, and LULC was a major control on the recharge lag time to hydroclimatic perturbations; recharge lag times were 20–24 months at irrigated sites and 5–31 years at rangeland sites. The historic total potential profile dynamics were most sensitive to location along the west–east gradient in average annual precipitation. Results also show that future recharge is greater under irrigated sites compared to rangeland sites along the west–east gradient. An important finding is that future total potential profiles were projected to have relatively more seasonal upward gradients under all LULCs, which explains the projected decrease in recharge rates by the mid- to late-21st century of more than 40% at some sites, particularly under RCP 8.5. These findings indicate that total potential profiles that control recharge rates may fundamentally change under future climate change across a range of LULC, which may further challenge the sustainability of some groundwater resources.

Keywords Recharge · Climate change · Groundwater recharge/water budget · Sustainability · Unsaturated zone

Introduction

Climate variability and change pose uncertainties for the sustainability of groundwater resources (Re et al. 2018; Gurdak 2017; Treidel et al. 2012; Green et al. 2011). Climate variability and change may result in more extreme periods of precipitation and drought; these changes in temperature and precipitation may in-turn affect recharge mechanisms and rates to local aquifers, particularly in semiarid and arid climates (Corona et al. 2018; Meixner et al. 2016; Taylor et al. 2012a). Recharge is one of the most important but challenging water budget components to quantify, particularly under projected future climate change (Green et al. 2011). A better understanding of the factors that affect recharge mechanisms and rates can improve current and future groundwater budgets and inform groundwater sustainability planning and related policy decisions.

Factors that affect natural recharge rates include land use/land cover (LULC), climate (precipitation, air temperature, relative humidity, etc.), and recharge mechanisms (Moeck et al. 2020). Diffuse and irrigation recharge mechanisms are the focus of this paper. Diffuse recharge is water from precipitation, including rain and snow, and irrigation recharge is irrigation return flow that infiltrates the land surface and flows through the vadose zone to reach the water table. Local, site-specific understanding of climate and subsurface geology is necessary when estimating recharge mechanisms due to spatial and temporal variability (McMahon et al. 2011). Interannual to multidecadal climate variability

✉ Jason J. Gurdak
jasongurdak@hotmail.com

[1] Department of Earth & Climate Sciences, San Francisco State University, San Francisco, CA, USA

[2] Department of Geosciences, University of Montana, Missoula, MT, USA

[3] Department of Geography & Environment, San Francisco State University, San Francisco, CA, USA

[4] Department of Civil, Environmental and Sustainable Engineering, Santa Clara University, Santa Clara, CA, USA

has also been shown to be an important control on recharge rates in many aquifer systems (Carvalho Resende et al. 2018; Velasco et al. 2017), including the High Plains aquifer (Kuss and Gurdak 2014), which is the study area of this research.

Diffuse recharge occurs beneath natural LULC and can be sensitive to changes in precipitation and air temperature (Moeck et al. 2020; Meixner et al. 2016), which affects evapotranspiration (ET), soil-water content, and most importantly the total potential gradients in the vadose zone that drives water movement and recharge (Gurdak et al. 2007). Here, recharge is evaluated that has intercepted the water table after water infiltrated through the soil and a downward flux through the vadose zone. Recharge that occurs from subsurface flow between hydrogeologic units is not a focus of this study.

In the vadose zone, water flows from areas of higher total potential to lower total potential (Wellings and Bell 1982). In some regions, particularly semiarid and arid climates, capillary and adsorptive forces of the soil matrix on water can cause either seasonal or persistent upward flow due to an upward total potential gradient towards land surface. Seasonal upward total potential gradients can occur during the summer or fall when ET rates increase (Wellings and Bell 1982; Fig. 1a). Persistent upward total potential gradients have been observed in some arid climates (Fig. 1b) and have developed over the geologic timescales (McMahon et al. 2003, 2006; Walvoord et al. 2004). Whether seasonal or persistent, upward total potential gradients can limit or prevent the downward flux of water through the vadose zone, which ultimately limits or prevents recharge. LULC and associated ET rates can influence the dynamics of total potential gradients, and thus are a potentially important controlling factor for recharge to an underlying aquifer. Vegetation rooting depth, wilting point, and fractional vegetation coverage are vegetation parameters that can alter ET rates and soil moisture, and thus total-potential gradient dynamics, and in turn, the timing and rates of recharge (Scanlon et al. 2005).

To date, few studies on the response of recharge to climate change have explored the underlying processes and mechanisms in thick vadose zones (Meixner et al. 2016). Moreover, no studies have explored how total potential gradients may respond to future climate change. This study explores these underlying processes and mechanisms and their response to climate change and variability.

Few studies have used field data from thick vadose zones to calibrate numerical models that evaluate climate variability and change effects on recharge in semiarid and arid aquifer systems such as the High Plains aquifer (Crosbie et al. 2013; Lauffenburger et al. 2018; Scanlon et al. 2003). A previous study by Lauffenburger et al. (2018) in the northern High Plains aquifer used different vadose zone monitoring sites and an ensemble of GCMs with Hydrus-1D to model two global warming scenarios, low warming (+1.0 °C) and high warming (+2.4 °C) for the year 2050. Projections of precipitation, irrigation requirements, ET, and diffuse and irrigation recharge rates for both warming scenarios at 2050 were compared to a baseline of 1990. The results showed no statistical difference in the low warming scenario of 2050 compared to 1990 but showed increased ET and irrigation requirements and decreased recharge in the high warming scenario. Statistical differences were also shown between the western and eastern sites and between rangeland and irrigated sites for both warming scenarios and the historic baseline (Lauffenburger et al. 2018). The west–east increasing trend in recharge rates is likely a response to the spatial patterns in average annual precipitation, which is a finding consistent with some previous studies (Crosbie et al. 2013; Szilagyi et al. 2011, 2013). However, the Lauffenburger et al. (2018) study did not evaluate the total potential gradients in the vadose zone and limited their study to evaluate recharge mechanisms.

The previously described knowledge gaps are addressed here by evaluating how the spatial and temporal patterns of natural recharge rates and mechanisms (diffuse and irrigation

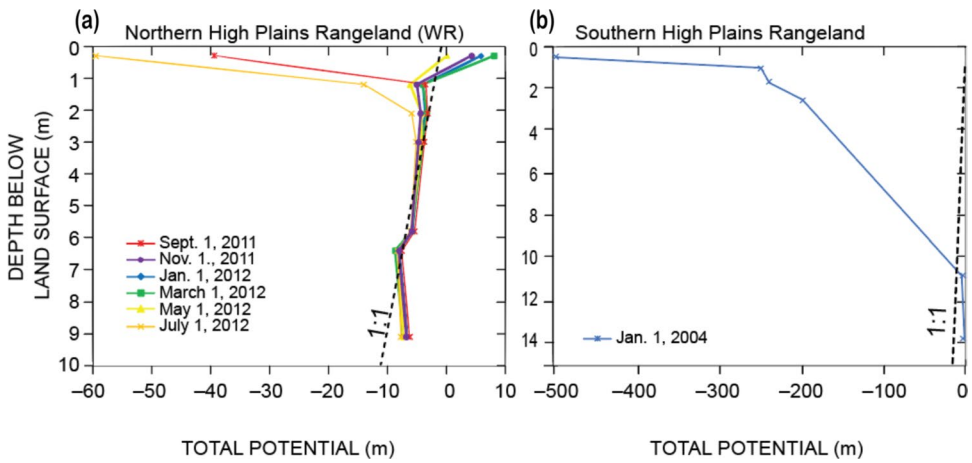

Fig. 1 **a** Seasonal fluctuations in total potential in northern High Plains rangeland (data modified from Steele et al. 2014). **b** Persistent upward total potential gradient in arid southern High Plains rangeland (data modified from Gurdak et al. 2007)

recharge) in thick vadose zones, ranging from 14 m to nearly 40 m, respond to a range of factors, including LULC and climate variability and change over the 21st century. A suite of long-term monitoring data from the vadose zone is used to calibrate Hydrus-1D (Šimůnek et al. 2008) models and run a series of scenarios to simulate historic and future projected recharge and systematically test the aforementioned factors. The models and scenarios will focus on the northern High Plains aquifer where an extensive dataset from the vadose zone is being collected (Gurdak et al. 2007; Lauffenburger et al. 2018; Steele et al. 2014). The High Plains aquifer is widely recognized as facing serious groundwater sustainability challenges (Smidt et al. 2016; Konikow 2013; Treidel et al. 2012).

Materials and methods

Study area

The study area is within the Central Platte Natural Resources District (CPNRD), which is located in central Nebraska overlying the northern High Plains aquifer (Fig. 2). The High Plains aquifer is one of the most stressed in the US and has large depletions in groundwater storage (Konikow 2013). The region is arid to semiarid with moderate precipitation and high evaporation (Gurdak et al. 2007). The High Plains aquifer is the largest groundwater resource in the central US and supports a large percentage of the country's irrigated grains (corn, wheat, and sorghum), but relies nearly 100% on groundwater to support this irrigated agriculture (Gurdak et al. 2009; McMahon et al. 2007). As a result of this dependency, the High Plains aquifer had the highest depletion rate of US aquifer systems in the 20th century (Konikow 2015). Due to strong spatial patterns in average annual precipitation and air temperature, the northern High Plains

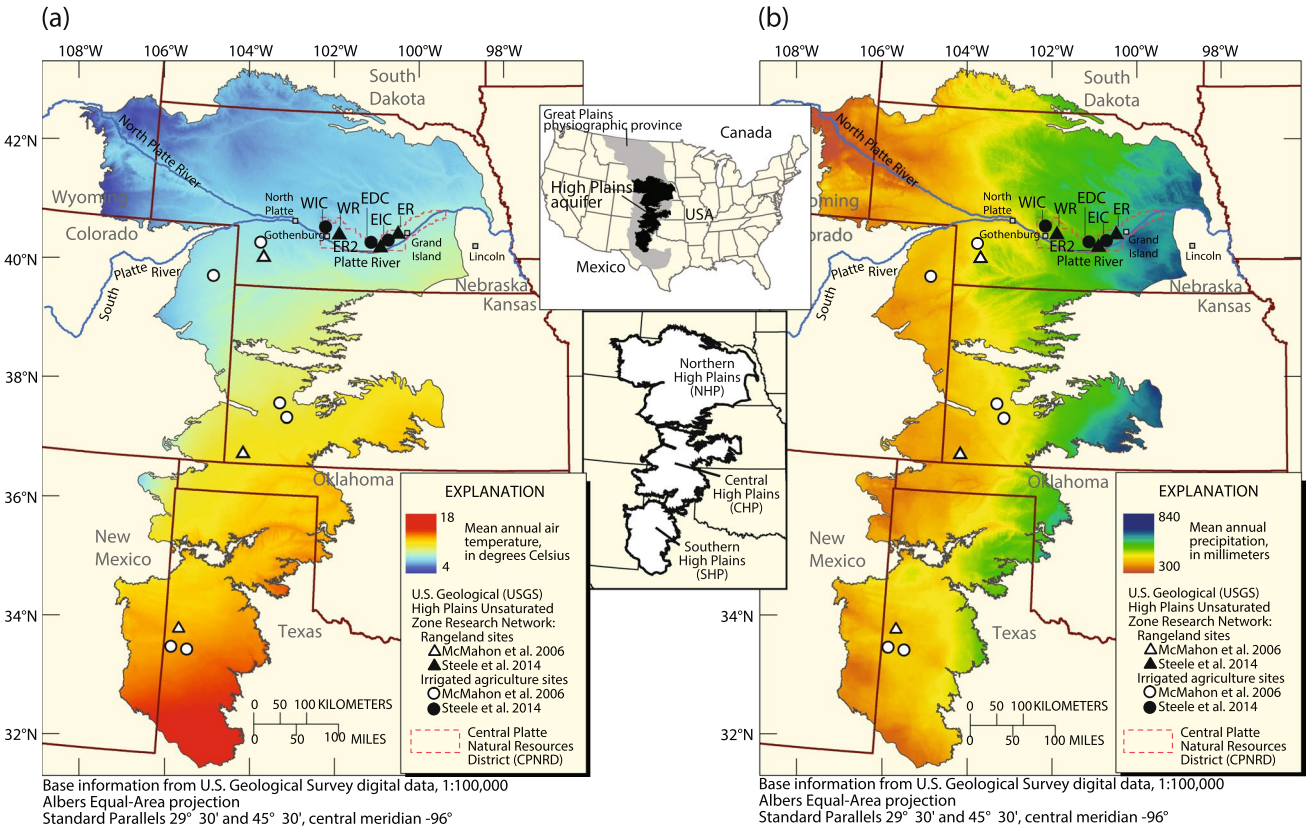

Fig. 2 Location of the northern High Plains rangeland and agricultural study sites on the distribution of regional **a** mean annual air temperature and **b** mean annual precipitation (modified from Lauffenburger et al. 2018 and McMahon et al. 2007). The study includes the western rangeland (WR), western irrigated corn (WIC), eastern rangelands (ER and ER2), eastern irrigated corn (EIC), and eastern dryland corn (EDC) sites in the Central Platte Natural Resources District (CPNRD). Air temperature and precipitation data credit to Thornton et al. (1997)

aquifer has some of greatest recharge rates of the entire aquifer system (Meixner et al. 2016; Konikow 2015; McMahon et al. 2006). Diffuse recharge is the primary mechanism in the northern High Plains aquifer, accounting for an estimated 85% of the total recharge (Meixner et al. 2016).

To evaluate factors that control the spatial and temporal patterns of natural recharge in thick vadose zones, such as LULC and historic and projected climate variability and change, a coordinated field and modeling approach was used at representative sites of the High Plains aquifer. The field sites and corresponding models are described and named as follows: western rangeland (WR), western irrigated corn (WIC), eastern rangeland (ER), eastern rangeland 2 (ER2), eastern irrigated corn (EIC), and eastern dryland corn (EDC; Table 1). The location of the six sites and the irrigated and rangeland LULC is shown in Fig. S1 of the electronic supplementary material (ESM). These six sites were selected because they represent diffuse and irrigated recharge settings in the most dominant LULC of the northern High Plains aquifer (Steele et al. 2014), as well as the west to east gradient in average annual precipitation (Fig. 2b). Historical annual data shows greater precipitation at the Grand Island meteorological station (eastern study area) than the Gothenburg meteorological station (western study area; NOAA 2018).

Recharge monitoring sites

Installation of the recharge monitoring sites took place between 2008 and 2010 and followed methods described in Gurdak et al. (2007); Lauffenburger et al. (2018); McMahon et al., (McMahon et al. 2003, 2006); and Steele et al. (2014). At each site, a 15-cm hollow-stem auger was used to drill a borehole down to the water table. During drilling, continuous soil-core samples from the vadose zone were collected using split-spoon core barrel methods as described by Steele et al. (2014). Soil texture information from the soil-core samples, including percent sand, silt, and clay and bulk density, were input into Hydrus-1D using the Rosetta Dynamically Linked Library to calculate water retention parameters and saturated hydraulic conductivity; those parameters were used to build the vadose zone strata columns for each model (Schaap et al. 2001; Šimůnek et al. 2008). The hydraulic properties and soil-water retention parameters for each layer in the Hydrus-1D models are listed in Table S1 of the ESM, including soil layers, depth interval below land surface, residual and saturated water content, parameters alpha and n from the soil-water retention function, saturated hydraulic conductivity, and tortuosity parameter.

At each site, a series of heat dissipation probes (HDPs) were installed within the boreholes at various depths, as described in Gurdak et al. (2007) and McMahon et al. (2003). The HDPs are used to measure in-situ matric potential (KPa) at 15-min intervals (Campbell Scientific Inc. 2009; Steele et al. 2014). The total potential at each HDP depth within the vadose zone is calculated as the sum of the observed matric potential values and the gravitational potential (m), using land surface as the datum. Osmotic potential is assumed negligible for these total potential calculations (McMahon et al. 2006). The calculated total potential time series were used during calibration of the Hydrus-1D models and validation of the simulated total potential gradients.

Hydrus-1D models

A Hydrus-1D (Šimůnek et al. 2008) model was created to represent each of the six monitoring sites and were used to simulate total potential gradients, water flux through the vadose zone, and recharge rates. Hydrus-1D is a numerical modeling software package that solves the Richards' equation (Richards 1931) for flow in one-dimensional (1D) variably saturated porous media:

$$\frac{\partial \theta}{\partial t} = \frac{\partial}{\partial x}\left[K\left(\frac{\partial h}{\partial x} + \cos\ \alpha\right)\right] - S \quad (1)$$

where h is the water pressure head, θ is the volumetric water content, t is time, x is the spatial coordinate, S is the sink term, α is the angle between the flow direction and

Table 1 Vadose zone monitoring sites used in this study. Note: the depth to water values were recorded at the time of well installation between 2008–2013, and depth to water minimum and maximum represents the range in groundwater levels from installation to 2021

Site	USGS site ID	Depth to water (bls, m)	Depth to water minimum and maximum (bls, m)	Land surface elevation (m)
Western rangeland (WR)	405738099504501	14.2	8.5–14.6	778
Western irrigated corn (WIC)	405855100073901	17.7	15.5–20.7	803
Eastern rangeland (ER)	410102098374201	20.2	19.5–22.3	607
Eastern rangeland 2 (ER2)	405435098432601	20.6	19.8–22.6	625
Eastern irrigated corn (EIC)	405855098383001	27.7	26.5–41.8	618
Eastern dryland corn (EDC)	405503098441801	38.9	38.1–41.1	647

Land surface elevation above sea level using the North American Vertical Datum of 1988; USGS site data available in the USGS National Water Information System (NWIS), USGS (2022)

bls below land surface; *m* meters

the vertical axis, and K is the unsaturated hydraulic conductivity function (Šimůnek et al. 2013). Simulated head values from the vadose zone and recharge rates from each model were analyzed to evaluate the controlling factors of recharge.

All six Hydrus-1D models use the van Genuchten-Mualem single porosity model with no hysteresis to represent the soil-moisture retention function (Šimůnek et al. 2013). The upper boundary of the models was defined as an atmospheric boundary condition with surface runoff and the lower boundary was near the bottom of the vadose zone based on depth to water during site installation (Table 1), and thus represents flow dominated by gravity and not influenced by water-table fluctuations. The range in depth to water at each site (Table 1) and water level hydrographs (Fig. S2 of the ESM) indicate the water table is generally lower than lower boundary of the model. Therefore, the simulated flux from the bottom of the model domain represents recharge to the water table.

The hydraulic parameters of the models are based on data collected from each of the six monitoring sites within the CPNRD (Fig. 2). Root water uptake was simulated for each Hydrus-1D model with parameters defined by Feddes et al. (1978) and specific values for corn and rangeland from Wesseling et al. (1991). The rangeland sites (ER, ER2, and WR) simulate ground cover of mixed-grass prairie plant species with a crop height of 2 m and rooting depth of 2.5 m, with a greater field observed root density in the upper 0.5 m below land surface (Lauffenburger et al. 2018). The corn sites (EIC, EDC, and WIC) simulate ground cover of seasonal corn crops, from late June to mid-September, with a maximum crop height of 2 m and rooting depth of 1.7 m, with greater field observed root density in the upper 0.5–1.0 m below land surface (Lauffenburger et al. 2018). Irrigation requirements were calculated for sites EIC and WIC. The models of the irrigated sites were first run with input from each GCM, which are described in the following sections. The Hydrus-1D model outputs of ET*, evaporation, transpiration, net shortwave radiation*, net longwave radiation*, radiation term*, aerodynamic term*, precipitation, interception, and excess interception (*terms calculated from the Penman-Monteith combination equation; Šimůnek et al. 2013) from each run were input into the Nebraska Department of Natural Resources Crops Simulation Model (CROPSIM) as outlined in Lauffenburger et al. (2018). CROPSIM uses these inputs to calculate irrigation requirements for corn crops during peak irrigation seasons from late June to mid-September of each year of the run. The calculated irrigation requirements were then added to precipitation inputs and the models were run again; outputs from the second run were then used for analysis for both irrigated sites.

Historical simulations and model spin-up

Historical climate data sets were compiled from the National Oceanic and Atmospheric Administration (NOAA) National Climatic Data Center (NCDC; NOAA 2018) to provide daily time series inputs of minimum and maximum air temperature and precipitation for the Hydrus-1D models to simulate recharge and total potential profiles for historic purposes. Eastern and western sites used NOAA historical data sets from Grand Island (sites: ER, ER2, EIC, and EDC) and Gothenburg (sites: WR and WIC) meteorological stations, respectively, based on their proximity to the sites. Simulated minimum and maximum air temperature and precipitation from a suite of GCMs were used as inputs in the models to simulate historic and future recharge. Potential evapotranspiration, referred to as ET here, was calculated by Hydrus-1D using the minimum and maximum air temperature as inputs in the Penman-Monteith combination equation (Šimůnek et al. 2013). Additional climate inputs of relative humidity (RH), wind speed, and radiation were collected from historical data from Lauffenburger et al. (2018), averaged for each day of the year, and repeated for every year of the run and used for every model.

Historical climate data from 1950 to 1980 were used in model spin-up simulations for each site. The purpose of a spin-up model is to address uncertainties in initial condition inputs inherent in modeling by running the model for a duration of time to achieve an equilibrium, either steady-state or dynamic, in soil-moisture content and temperature (Ajami et al. 2014; Seck et al. 2015). Once equilibrium is reached, soil-moisture outputs are then used as the initial condition inputs in the model intended for the study to effectively simulate integrated hydrologic systems (Seck et al. 2015). For this study, spin-ups were run for each site's model using historical NOAA climate data from 1950–1980 to achieve equilibrium in soil-moisture contents of the vadose zone profile. Spin-up outputs of the soil-moisture profile were then used as the initial water content conditions of the subsequent model runs.

Model assumptions

The Hydrus-1D models are numerical representations of six study sites located in the CPNRD, and a few assumptions were made to simplify the natural complexity of the interactions between the atmosphere, vadose zone, and water table. First, the thickness of the vadose zone is assumed to be constant with time; depth to the water table at the time of well installation for each site was used as the vadose zone thicknesses ranging from 14.2 to 38.9 m. Therefore, simulated bottom flux is assumed to represent recharge flux to the water table. The model also uses daily relative humidity, wind speed, and radiation that are repeated for each

year of the simulation because forecasts of these data are not readily available. It is assumed that the LULC for each model is constant over time. In reality, agricultural expansion occurs where rangeland is converted to cropland and irrigation practices can evolve and change over time (Scanlon et al. 2005), and future changes in LULC in response to projected climate change are unknown. Finally, because data from site-specific cores are used to calibrate Hydrus-1D models, the representative spatial scale of recharge beneath each site-specific model is on the order of 1–10 m^2 (Healy 2010). Additionally, it was assumed that each site-specific model is generally representative of recharge beneath similar LULC across the northern High Plains aquifer, which is a well documented field and modeling approach to understanding recharge processes in the vadose zone (McMahon et al. 2003, 2006; Gurdak et al. 2007; Steele et al. 2014; Lauffenburger et al. 2018; Moeck et al. 2020).

Model calibration

To calibrate the models, a trial-and-error approach was used for history matching, which included qualitative and quantitative methods to compare simulated and observed total potential values from the HDPs below the root zone that were collected between 2008 and 2017. During the model calibration, the thickness of the model layers and cell discretization of the models were adjusted to improve the calibration fit rather than adjust hydraulic parameters of individual model layers, which were based on soil core texture and associated hydraulic properties. The qualitative calibration method involved visually comparing the simulated and observed total potential profiles below the root zone. In general, the calibrated models provide a reasonable simulation of the seasonal dynamics in the total potential profiles observed at the six sites. The quantitative calibration method relied on the commonly used Nash-Sutcliffe coefficient of efficiency (NSE) (Anderson et al. 2015). Given the high temporal variability in total potential values in the near surface, the NSE was calculated using monthly average observed and simulated total potential vertical gradients (slopes) below the root zone to evaluate model calibration of water flux in the vadose zone below the zero-flux plane, which is often near the base of the root zone (Healy 2010). Examples of the monthly average observed and simulated total potential vertical gradients (slopes) are shown in Fig. S3 of the ESM. The NSE was calculated as:

$$\mathrm{NSE} = \frac{\sum_{i=1}^{n} \left| \left(X_{\mathrm{t,m}} - X_{\mathrm{t,s}} \right) \right|_i^2}{\sum_{i=1}^{n} \left| \left(X_{\mathrm{t,m}} - \overline{X}_{\mathrm{t,m}} \right) \right|_i^2} \tag{2}$$

where $X_{\mathrm{t,m}}$ is the measured (observed) total potential slope, $X_{\mathrm{t,s}}$ is the simulated total potential slope, and $\overline{X}_{\mathrm{t,m}}$ is the mean of the measured total potential slope. NSE values range from $-\infty$ to 1, where values close to 1 indicate a good fit (Anderson et al. 2015). For NSE values of 0, the mean of the data is as good a predictor as the simulated values; and for a value less than 0, the mean of the data would be a better predictor (Anderson et al. 2015). The calculated NSE values range from –2.76 to 0.81 and indicate a reasonably good fit between the simulated and observed total potential vertical gradients.

NOAA climate data from 2008 to 2017 were used as meteorological model inputs because this coincides with the period of data collection at the six sites. The Hydrus-1D models were built with simulated observation nodes in the model profile at the same depths as the HDPs in the vadose zone of each site. Hydrus-1D was used to simulate a time series of hydraulic head, in meters, at the depth for each observation node for the duration of the model run. Total potential time series for each model observation node were calculated by summing the absolute value of simulated head values and the gravitational potential at each observation node. Generally, total potential is calculated by summing matric potential and the gravitational potential, which is the elevation of the observation point above a chosen reference datum; for the Hydrus-1D observation nodes, head outputs are used as the matric potential values (Radcliffe and Šimůnek 2010; Wellings and Bell 1982). Ground level was chosen as the reference datum, which causes the gravitational potential values to be negative. The Hydrus-1D simulated observation node and calculated HDP total potential field data were given in inconsistent timesteps, so all total potential time series were processed to achieve average daily and monthly time series for calibration purposes. Monthly total potential profile of the vadose zone calculated from model outputs and observed field data; the slopes of the profiles below the rooting zone were visually compared to calibrate each model. Generally, the total potential slopes from the observed data varied more than the simulated total potential vertical gradients, but looked similar overall and provided qualitative support regarding the reasonable NSE values for the model calibration.

Simulated future recharge under climate change

To simulate future recharge, projected precipitation and temperature for the sites were used via downscaled climate model data for the years 1950 to 2100. Future projections were based on output from global climate model (GCM) simulations conducted as part of the Coupled Model Intercomparison Project - Phase 5 (CMIP5; Taylor et al. 2012b). The CMIP5 experiments formed the basis for the climate model simulations included in the 5th assessment of the

Intergovernmental Panel on Climate Change (Stocker 2014). The GCMs used in this study are listed in Table 2. These GCMs were selected based on the availability of complete daily precipitation and temperature data for both a historical period and future projections and available output for both a higher emissions pathway—representative concentration pathways (RCP) 8.5—and a lower emissions pathway (RCP 4.5). RCP 4.5 is a global climate projection scenario where total global radiative forcing stabilizes by 2040 due to policies, strategies, and technologies expected to be enacted to reduce greenhouse gas emissions (Clarke et al. 2007; Smith and Wigley 2006; Wise et al. 2009). RCP 8.5 is a scenario where greenhouse gas emissions continue to increase at the same rate as is happening currently without any strategies employed to decrease emissions (RCP Database 2009; Riahi et al. 2007). It should be noted that the use of the term 'historical' here refers to recharge modeling from 1950–2009, which is not exactly the same as the historical period (1950–2005) used by the CMIP5 climate modeling experiments. This difference in terminology does not affect the modeling results.

Eight of these nine GCMs were included in a previous study (Polade et al. 2013) that demonstrated successful simulation of important teleconnections between oceanic oscillations, such as El Niño/Southern Oscillation (ENSO) and Pacific Decadal Oscillation (PDO), and North American precipitation, which are important features for this study. An ensemble of nine GCMs is large enough where characterization of the ensemble mean and variability tends to be relatively insensitive to the individual selection of GCMs (Maurer et al. 2014), and using an ensemble of GCMs is consistent with guidance from previous climate-impact recharge studies (Lauffenburger et al. 2018; Crosbie et al. 2011; Holman et al. 2011).

The GCM output was statistically downscaled to a fine 1/16° (approximately 6 km) spatial resolution producing daily precipitation and temperature (maximum and minimum) using the localized constructed analogs method (LOCA) (Pierce et al. 2014). The LOCA method was developed to maintain specific hydrologically important characteristics including spatial correlations of events and low-frequency variability, and has been incorporated in a publicly available dataset of downscaled data (Bracken 2016). The LOCA method uses an analog matching algorithm to downscale large-scale GCM output to fine scales, ensuring that the daily downscaled fields of precipitation and minimum/maximum temperature are consistent on both the regional and local spatial scales. LOCA begins by correcting the annual cycle so that both the GCM and observations display the same seasonality in both temperature and precipitation. Using a seasonal window, the distributions of precipitation and temperature are corrected using methods similar to quantile mapping (Li et al. 2010) for temperature and the PresRat (Pierce et al. 2015) method for precipitation. A frequency-dependent bias correction (Pierce et al. 2015) is then applied to the time series, adjusting the amplitude of GCM variability in frequency bands from 2 days to 11 years to better match the observations. Finally, the downscaling procedure begins by establishing coarse resolution analog points with a defined surrounding region with positively correlated meteorology. An analog day is selected from the historical record, and the final downscaled field is constructed by scaling the fine-scaled observations, at 1/16° for this application, for that day to match bias-corrected GCM meteorology.

Each Hydrus-1D model was run with LOCA downscaled precipitation and minimum and maximum air temperature output from each GCM. Therefore, the total ensemble of Hydrus-1D output for each of the six sites includes 18 model scenarios (nine GCMs each at RCP 4.5 and 8.5). The primary Hydrus-1D output analyzed here was the daily simulated bottom flux (recharge) from each of the 18 model scenarios for the years 1950–2100 and head at depth from the CANESM2 GCM at RCP 4.5 and 8.5 used to calculate

Table 2 Ensemble of global climate models (GCMs) used in this study

Abbreviation	Organization
CANESM2	Canadian Centre for Climate Modelling and Analysis
CNRM-CM5	Centre National de Recherches Météorologiques/Centre Européen de Recherche et Formation Avancée en Calcul Scientifique
CSIRO-MK3-6-0	Commonwealth Scientific and Industrial Research Organization in collaboration with Queensland Climate Change Centre of Excellence
GFDL-ESM2G	NOAA Geophysical Fluid Dynamics Laboratory
INMCM4	Institute for Numerical Mathematics
MIROC5	Atmosphere and Ocean Research Institute (The University of Tokyo), National Institute for Environmental Studies, and Japan Agency for Marine-Earth Science and Technology
MPI-ESM-LR	Max-Planck-Institut für Meteorologie (Max Planck Institute for Meteorology)
MRI-CGCM3	Meteorological Research Institute
NORESM1-M	Norwegian Climate Centre

simulated future total potential profiles for the years 2040 and 2099. CANESM2 was used to simulate the total potential profiles because this GCM is approximately average in terms of projected precipitation and temperature from the nine GCMs.

Simulated historical recharge under climate variability

To evaluate the effects of climate variability on recharge, historical recharge and total potential profiles in the vadose zone for each of the six were simulated using Hydrus-1D site models and compared the outputs to historical periods of above-average precipitation and drought (wet and dry periods). Historical precipitation and minimum and maximum air temperature data for the years 1950–2018 were compiled from two long-term meteorological stations in Gothenburg, NE and Grand Island, NE (NOAA 2018) to represent the precipitation and air temperature at the western and eastern sites, respectively. A long-term (2005–2018) time series of the monthly Palmer Drought Severity Index (PDSI) from the South-Central Climate Division of Nebraska (NOAA 2021) was used to evaluate recharge response to wet and dry periods. Based on the monthly PDSI (NOAA 2018), five from each of the most recent and prominent wet and dry periods for the study area were chosen. Dry periods are indicated by negative PDSI values and wet periods are indicated by positive PDSI values. A time series of simulated recent historic recharge rates for each site was visually compared and statistically correlated to a time series of PDSI values as well as a phase lag time correlation of historic recharge time series to PDSI values using HydroClimATe: Hydraulic and Climatic Analysis Toolkit (Dickinson et al. 2014). HydroClimATe was used to calculate time lag correlations (95% confidence interval) of historic recharge time series to PDSI values for each site for time lags of 1–414 months. The monthly phase lag with the highest correlation coefficient for each site was determined and used to compare a phase-adjusted time series of historic recharge to PDSI values. Daily snapshots of total potential profiles for the most recent wet and dry periods were used to evaluate the effects of climate variability on total potential profiles.

Statistical analyses

The Kruskall-Wallis nonparametric test with an alpha level (α) of 0.05 was used to determine differences between the non-parametric groups of data (Helsel and Hirsch 1992). Subsequently, the Steel-Dwass All Pairs test, which is equivalent to the non-parametric version of the Tukey test was used to determine differences among the groups of data (JMP 2010). These statistical tests were used to analyze the differences between historical and future simulated values, the six sites, and RCP 4.5 and 8.5.

Results and discussion

The results of the simulated historical (1950–2009) and future (2010–2100) precipitation, ET, irrigation requirements, and recharge at each of the six sites using the 18 GCM model scenarios are shown in Figs. 3, 4, 5 and 6, respectively. To evaluate future changes in recharge over the 21st century, the results in Figs. 3, 4, 5 and 6 are presented for the following future time periods: 2010–2039, 2040–2069, and 2070–2099. The effects of the west–east gradient in average annual precipitation (western, W) and eastern, E) and LULC (rangeland, R), irrigated cornland, IC), and dryland corn, DC) are also shown in Figs. 3, 4, 5 and 6, as well as in Figs. 7 and 8, which show recharge response to historical climate variability and Figs. 9, 10 and 11, which show historic and future total potential profile dynamics. The results are discussed in the next section.

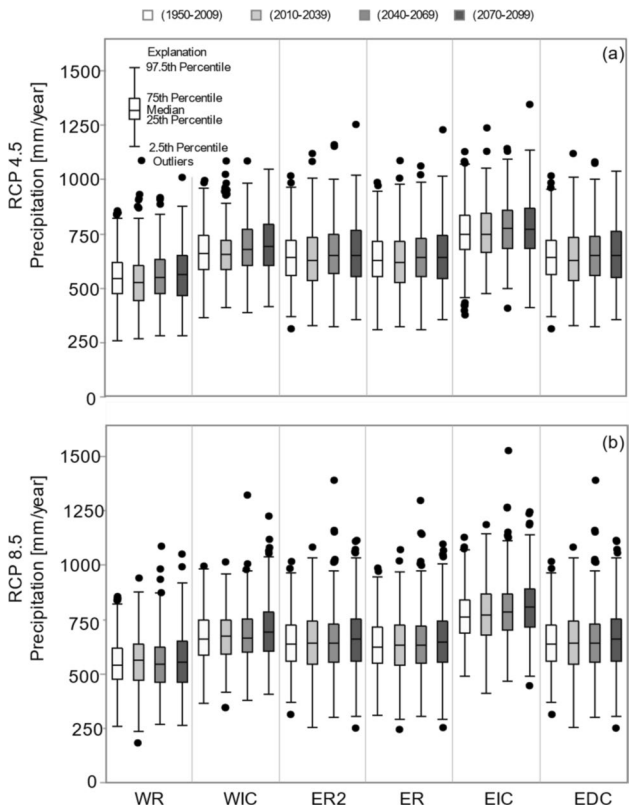

Fig. 3 Simulated historic (1950–2009) and future (2010–2100) precipitation (mm/year) at each of the six study sites—western rangeland (WR), western irrigated corn (WIC), eastern rangeland (ER), eastern rangeland 2 (ER2), eastern irrigated corn (EIC), and eastern dryland corn (EDC)—based on LOCA downscaled output from nine GCMs using **a** RCP 4.5 and **b** RCP 8.5

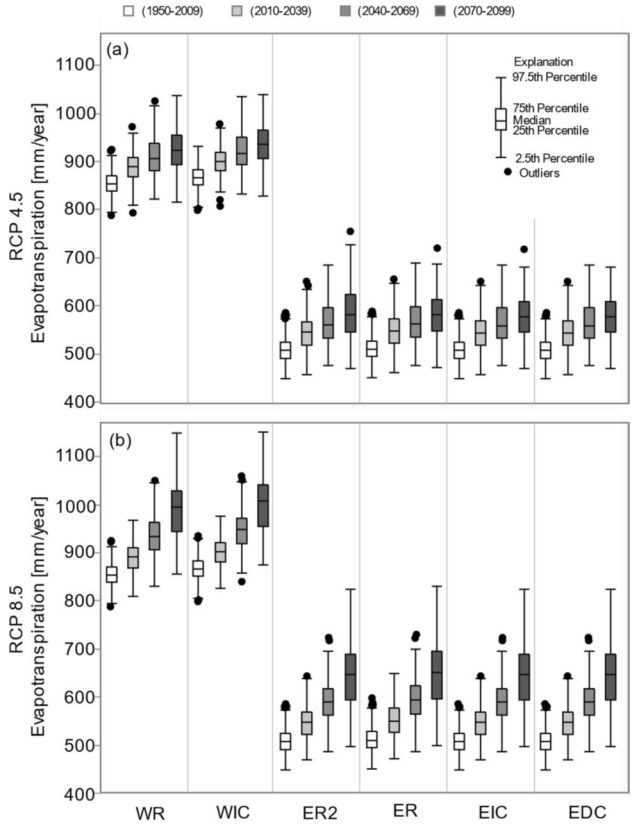

Fig. 4 Simulated historic (1950–2009) and future (2010–2100) evapotranspiration (ET) (mm/year) from Hydrus-1D at each of the six study sites—western rangeland (WR), western irrigated corn (WIC), eastern rangeland (ER), eastern rangeland 2 (ER2), eastern irrigated corn (EIC), and eastern dryland corn (EDC)—based on LOCA downscaled output from nine GCMs using **a** RCP 4.5 and **b** RCP 8.5

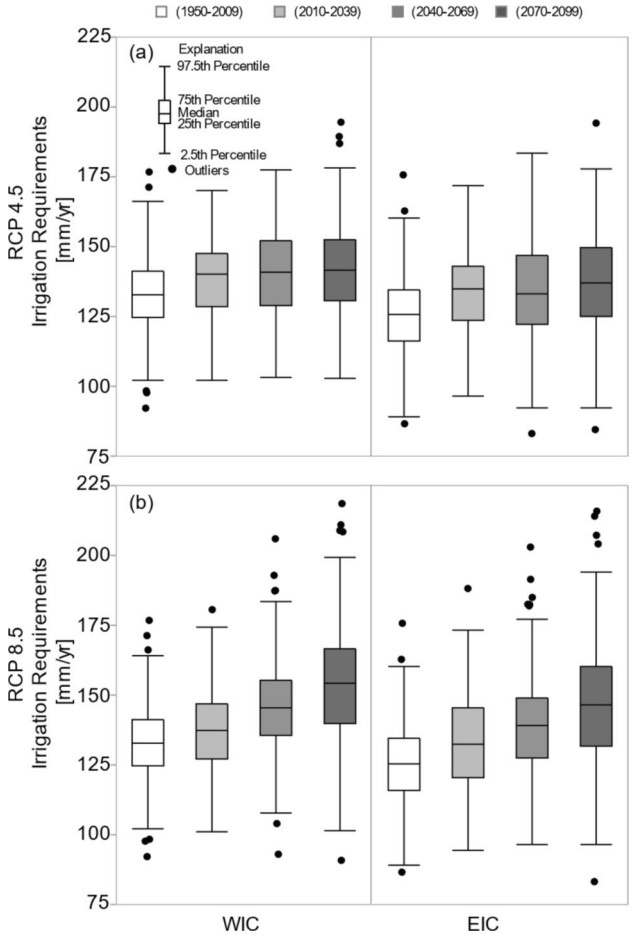

Fig. 5 Simulated historic (1950–2009) and future (2010–2100) irrigation requirements (mm/year) from Hydrus-1D at each both irrigated corn sites—western irrigated corn (WIC), eastern irrigated corn (EIC)—based on LOCA downscaled output from nine GCMs using **a** RCP 4.5 and **b** RCP 8.5

Precipitation trends

Precipitation outputs from the nine GCMs and RCP 4.5 and 8.5 ranged from 183 to 1,528 mm/year across all sites (Fig. 3). Under both RCP 4.5 and 8.5, most of the six sites have an increase in the median precipitation from the historical (1950–2009) to late-21st century (2070–2099; Fig. 3) based on the Steele-Dwass test (α-level = 0.05).

Under RCP 4.5, comparisons of time periods for each site showed precipitation for historical (1950–2009), early-21st century (2010–2039), mid-21st century (2040–2069), and late-21st century (2070–2099) were not statistically different at sites WR, ER, ER2, EIC, and EDC. Site WIC indicated statistically significant differences in precipitation between late-21st (2070–2099) and both historic (1950–2009) (p value = 0.011) and early-21st century (2010–2039) (p value = 0.002). Comparisons of precipitation in each of the time periods under RCP 4.5, precipitation for all sites for the historical (1950–2009) and early-21st century (2010–2039) are not statistically different (p value=0.184) and similarly, the mid- (2040–2069) and late-21st century (2070–2099) are not statistically different (p value = 0.919). These results indicate a statistical difference in median precipitation between early- and mid-21st century, but the median precipitation remains relatively constant between the mid- and late-21st century.

Under RCP 8.5, comparisons of time periods for each site showed precipitation was not statistically different over time at the nonirrigated sites (WR, ER, ER2, and EDC). Sites WIC and EIC indicated statistical differences between greater median precipitation in the late-21st (2070–2099) as compared to this historical period (1950–2009) (p value = 0.007 and 0.001 respectively). Under RCP 8.5, precipitation for the late-21st century (2070–2099) was statistically different than precipitation for both historic (1950–2009) and early-21st century (2010–2039) time periods (p value <0.001 and 0.024 respectively) for all sites.

Comparing precipitation in the western sites (WR and WIC) to the eastern sites (ER, ER2, EIC, and EDC), under

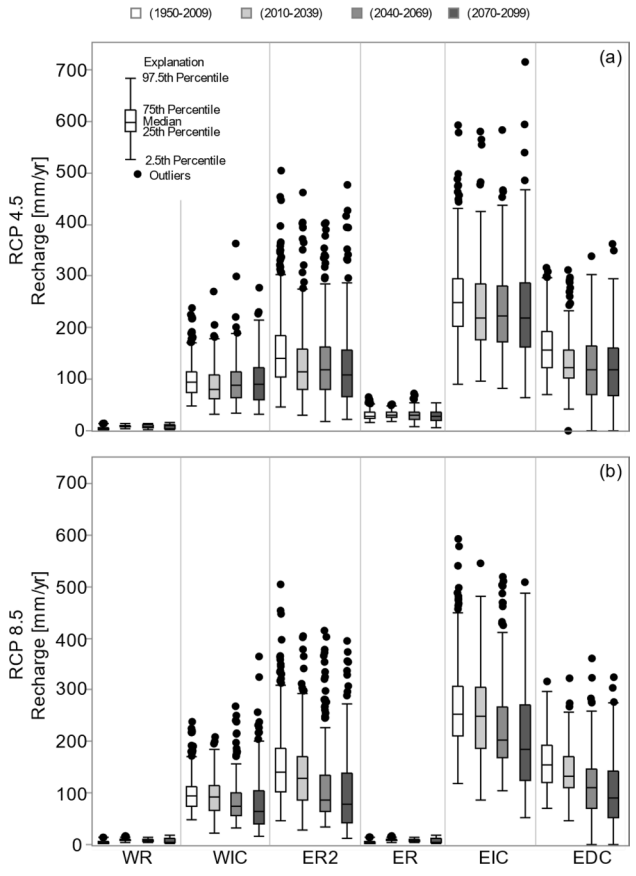

Fig. 6 Simulated historic (1950–2009) and future (2010–2100) recharge (mm/year) from Hydrus-1D at each of the six study sites—western rangeland (WR), western irrigated corn (WIC), eastern rangeland (ER), eastern rangeland 2 (ER2), eastern irrigated corn (EIC), and eastern dryland corn (EDC—based on LOCA downscaled output from nine GCMs using **a** RCP 4.5 and **b** RCP 8.5

both RCPs 4.5 and 8.5, the western sites (WR and WIC) have significantly lower (p value < 0.001) median precipitation than the eastern sites (ER, ER2, EIC, and EDC). The results of these statistical tests confirm the visual west-east precipitation gradient among the sites (Fig. 2).

Evapotranspiration trends

ET was calculated as Hydrus-1D simulation outputs for each GCM, RCP, and site and ranged from 448 to 1,150 mm/year (Fig. 4). ET increased over time for each site and RCP, with more pronounced increases under RCP 8.5 (Fig. 4). Under both RCP 4.5 and 8.5, ET at each of the six sites was statistically greater during each subsequent time period (Steele-Dwass, p-value range <0.001–0.002).

Under RCP 4.5, there were no significant spatial differences in ET values among any of the eastern sites (ER, ER2, EIC, and EDC) during similar time periods (Steele-Dwass, p-value range = 0.339–0.999). There were statistical differences between both western sites during similar time periods (WR and WIC) (p-values <0.001).

Similarly, under RCP 8.5 there were no significant spatial differences in ET values among any of the eastern sites (ER, ER2, EIC, and EDC) during similar time periods (p-value range = 0.341 to 0.999). Under the late-21st century time period, both western sites (WR and WIC) had no statistical difference in ET as well (Steele-Dwass, p-value = 0.2142). However, there were statistical differences in ET values between both western sites (WR and WIC) during the historical to mid-21st century periods; Steele-Dwass, p-values <0.001).

Comparing western to eastern sites, western sites have significantly greater ET values (Fig. 4). The simulated ET at western sites range from 788 to 1,150 mm/year, while eastern sites range from 448 to 830 mm/year.

Irrigation trends

Irrigation requirements were calculated using Hydrus-1D outputs in CROPSIM as described earlier for sites WIC and EIC (Fig. 5). There are no significant spatial differences in irrigation requirements between sites WIC and EIC under RCPs 4.5 and 8.5 during the historical (1950–2009) and early-21st century (2010–2039) time periods (Steele-Dwass, p-value range = 0.269–0.961). However, the two irrigation sites have statistical differences in irrigation requirements between RCPs 4.5 and 8.5 during the mid-21st century (2040–2069) and late-21st century (2070–2099) time periods, with larger irrigation requirements indicated in RCP 8.5 (Steele-Dwass, p-value range <0.001–0.005). Under each RCP and time period, irrigation requirements for sites WIC and EIC were statistically different, with WIC requiring more irrigation than EIC (Steele-Dwass, p-value range <0.001–0.004). These results reflect the precipitation gradient in the CPNRD where the western side of the study area has lower annual precipitation (Fig. 2b).

Future recharge trends

The simulated recharge ranged from 0 to 715 mm/year for the years 1950–2100 using the nine GCMs, RCPs of 4.5 and 8.5, and across all six study sites (Fig. 6). Under both RCP 4.5 and 8.5 and at most of the six sites, the simulated median recharge was statistically lower (Steele-Dwass, p-value < 0.05) by the middle (2040–2069) to late (2070–2099) 20th century as compared to the historical period (1950–2009) (Fig. 6). Because the spatial and temporal patterns of simulated recharge are generally very similar for both RCP 4.5 and 8.5 (Fig. 6a and b), the following presentation and discussion of results will focus on simulated recharge patterns under RCP 8.5.

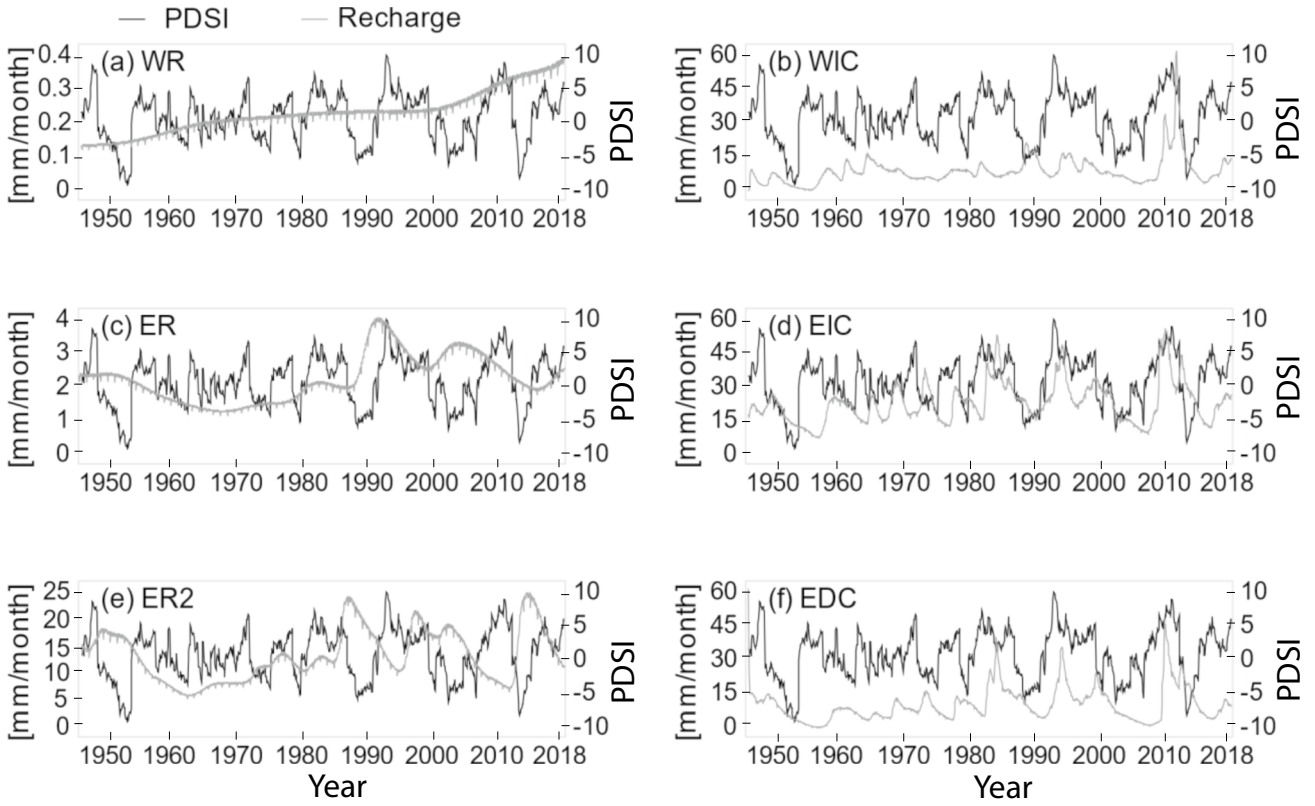

Fig. 7 Simulated historic recharge (mm/month) from Hydrus-1D (left y-axis) with PDSI values (right y-axis) to show peak wet and dry periods over the period 1950–2018 for sites **a** western rangeland (WR), **b** western irrigated corn (WIC), **c** eastern rangeland (ER), **d** eastern irrigated corn (EIC), **e** eastern rangeland 2 (ER2), and **f** eastern dryland corn (EDC)

Each of the six sites had statistically different simulated median recharge rates during the historic period under RCP 8.5 (Steele-Dwass, p-value <0.001), with the exception of sites WR and ER that had no significant differences detected in historic recharge rates (Fig. 6b). During the historical period, the greatest recharge rates were beneath the EIC, EDC, ER2, and WIC sites, respectively. The historical recharge rates beneath the WR and ER sites were about 100 mm/year lower or more than the corresponding irrigated sites, as described in the following. During the historical period, the simulated recharge beneath the western sites (WR and WIC) was statistically lower than beneath the eastern sites (ER, ER2, EIC, and EDC), based on results of the Kruskal-Wallis test (p-values <0.001). These east–west spatial patterns in simulated recharge rates are a response to substantially higher ET in the western sites compared to the eastern sites (Fig. 4). The relatively lower precipitation and higher ET at the western sites limits the soil moisture below the root zone that eventually becomes recharge.

All six sites except for WIC and EIC have simulated median recharge rates by the early-21st century (2010–2039) that are statistically lower by as much as 15% compared to the historical period under RCP 8.5 (Fig. 6b). By the middle (2040–2069) and for the late (2070–2099) 20th century, all six sites have statistically lower median recharge by more than 40% compared to the historical period (p-value range <0.001–0.008) (Fig. 6b). These forecasted decreases in future recharge rates are a response to the increased radiative forcings under RCP 8.5 that generally increase ET (Fig. 4b) and irrigation requirements (Fig. 5b) during the latter half of the 21st century.

All LULCs types (rangeland, irrigated corn, and dryland corn) for each time period have statistically different recharge rates (Steele-Dwass, p-value <0.001) under RCP 8.5, with the exception of irrigated corn sites (WIC and EIC) and the dryland corn site (EDC) during the historic (1950–2009) and early-21st century (2010–2039) time periods (Steele-Dwass, p-value range = 0.096–0.916). Although both ER and ER2 sites are rangeland sites in the eastern part of the study area, site ER2 has statistically greater recharge than ER for all time periods (Fig. 6b). The factors controlling these differences in recharge rates beneath LULC are explained using their respective total potential profiles in the following sections.

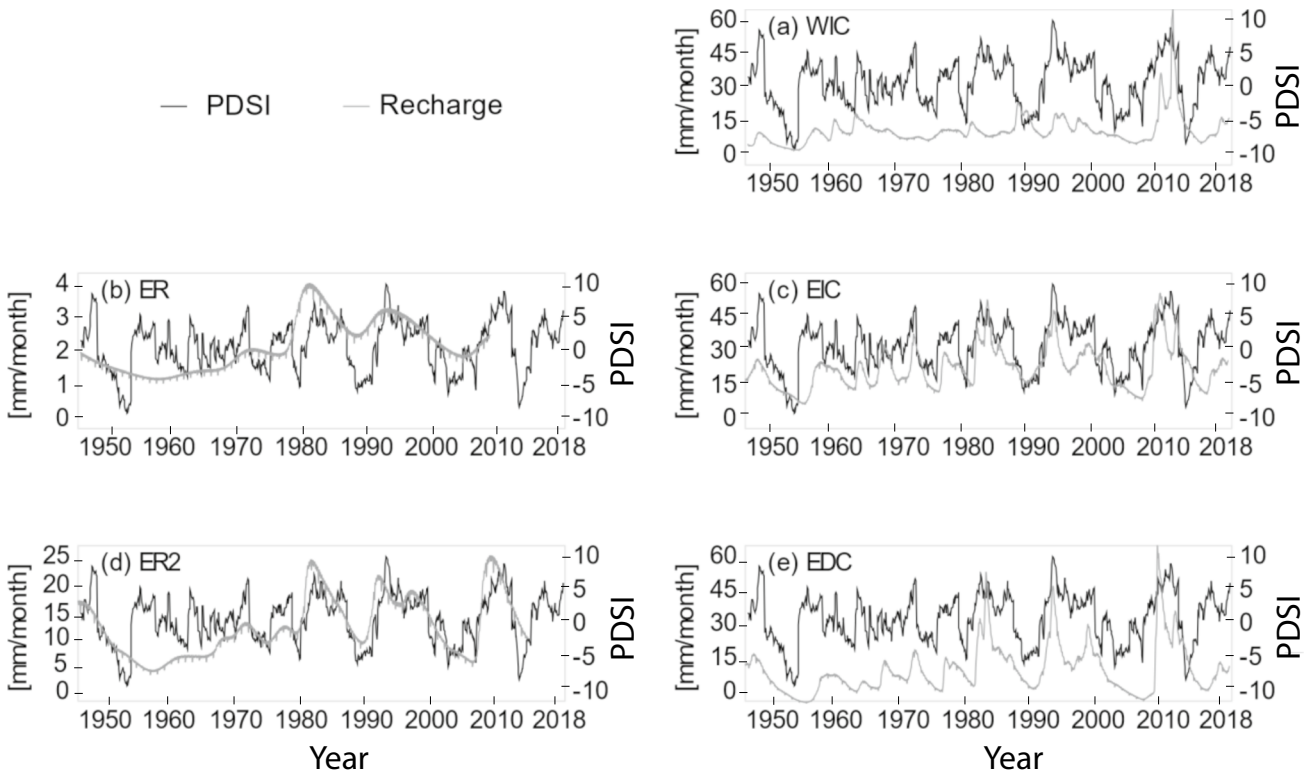

Fig. 8 Simulated historic recharge (mm/month) from Hydrus-1D (left y-axis) with PDSI values (right y-axis) adjusted with lag correlations over the period 1950–2018 for sites, **a** western irrigated corn (WIC) with a lag time of 24 months, **b** eastern rangeland (ER) with a lag time of 108 months, **c** eastern irrigated corn (EIC) with a lag time of 22 months, **d** eastern rangeland 2 (ER2) with a lag time of 58 months, and **e** eastern dryland corn (EDC) with a lag time of 20 months

Historic recharge trends with climate variability

To further evaluate recharge response to hydrologic extremes associated with climate variability, the time series of the PDSI was compared to the simulated recharge rates at the six sites over the historical period of 1950–2018 (Fig. 7). The PDSI and recharge time series have similar timing of relatively high and low values at the western and eastern irrigated and dryland corn sites (WIC, EIC, and EDC; Fig. 7b,d and f). These figures indicate that recharge beneath corn crops, regardless of irrigation, is relatively more responsive to wet and dry periods than the rangeland sites. Rangeland sites have very few, if any, similarities between the temporal variability phases of minimum and maximum PDSI and recharge time series and have opposing phases in some cases (Fig. 7a,c and e). Rangeland sites also showed pronounced seasonal dips in recharge compared to both irrigated and dryland corn crop sites. Although there appears to be some similarities between the PDSI and recharge time series at the irrigated sites, none of the six sites have statistically significant correlations (bivariate normal ellipse with a confidence of 0.95) between PDSI and recharge.

Given the time lag between any climate perturbation at land surface that affects ET and infiltration and the subsequent water flux downward through the vadose zone before recharging the water table, lag correlations were evaluated between the PDSI and simulated historical recharge time series. The lag time with the highest correlation coefficient for each site (Table 3) was then used to plot the phase-shifted simulated historic recharge time series against the PDSI value time series (Fig. 8). Site WR is omitted from Fig. 8 because no statistically significant lag correlation coefficients were detected within 30 years of phase lags, which is beyond the likely travel time of water flux though the vadose zone at this site. Visual examination of the phase-shifted recharge time series (Fig. 8) indicate a much closer response to PDSI for most sites, especially in terms of large positive PDSI values and large recharge values. The simulated recharge at the corn crop sites has moderate lag correlation coefficients to PDSI with similar phase lag times of 20–24 months (Table 3). The recharge beneath the eastern rangeland sites (ER and ER2) has a much slower response to PDSI with phase lag times of 108 and 58 months, respectively. These lag correlation results are consistent with LULC acting as an important

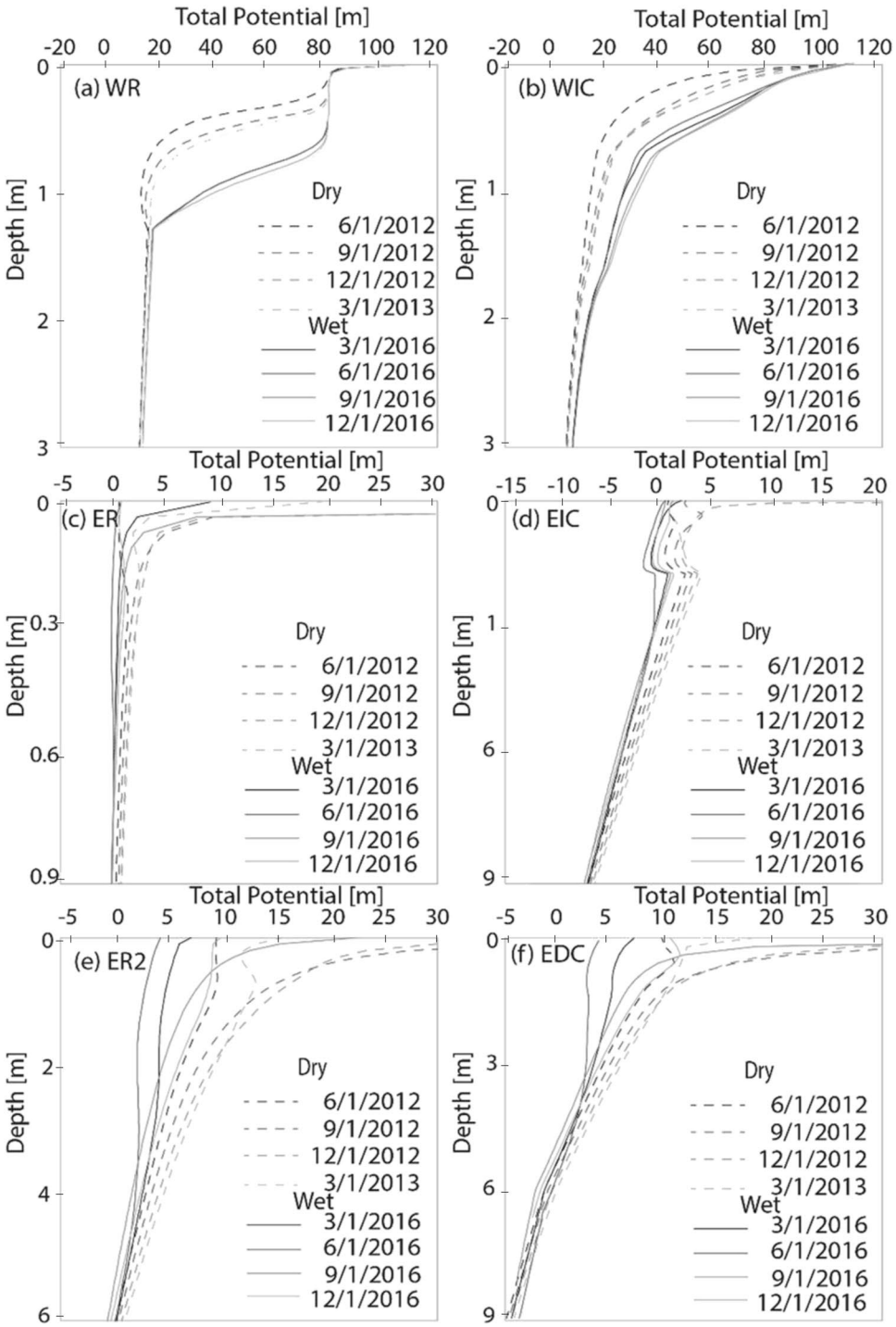

Fig. 9 Recent historical total potential profiles of calculated from Hydrus-1D head at depth output at sites **a** western rangeland (WR), **b** western irrigated corn (WIC), **c** eastern rangeland (ER), **d** eastern irrigated corn (EIC), **e** eastern rangeland 2 (ER2), and **f** eastern dryland corn (EDC). The dashed lines represent profiles centered on the most recent dry period in central Nebraska and solid lines represent profiles centered on the most recent wet period in central Nebraska. The top several meters are shown to highlight the variability in this part of the vadose zone. Dates given as mm/dd/yyyy

filter that influences the temporal responses in recharge to climate variability.

Using the PDSI, ten historical wet and dry periods were selected based on length and severity of the wet/dry period and compared to the median recharge at each site (Table 4). In general, the median recharge (mm/month) for each site is relatively greater under wet periods (positive PDSI values) and lower under the dry periods (negative PDSI values; Table 4). Recharge rates are statistically different between the wet and dry conditions for each site (Steele-Dwass, p-values = (ER) 0.006 and (WR, WIC, ER2, EIC, EDC) <0.001).

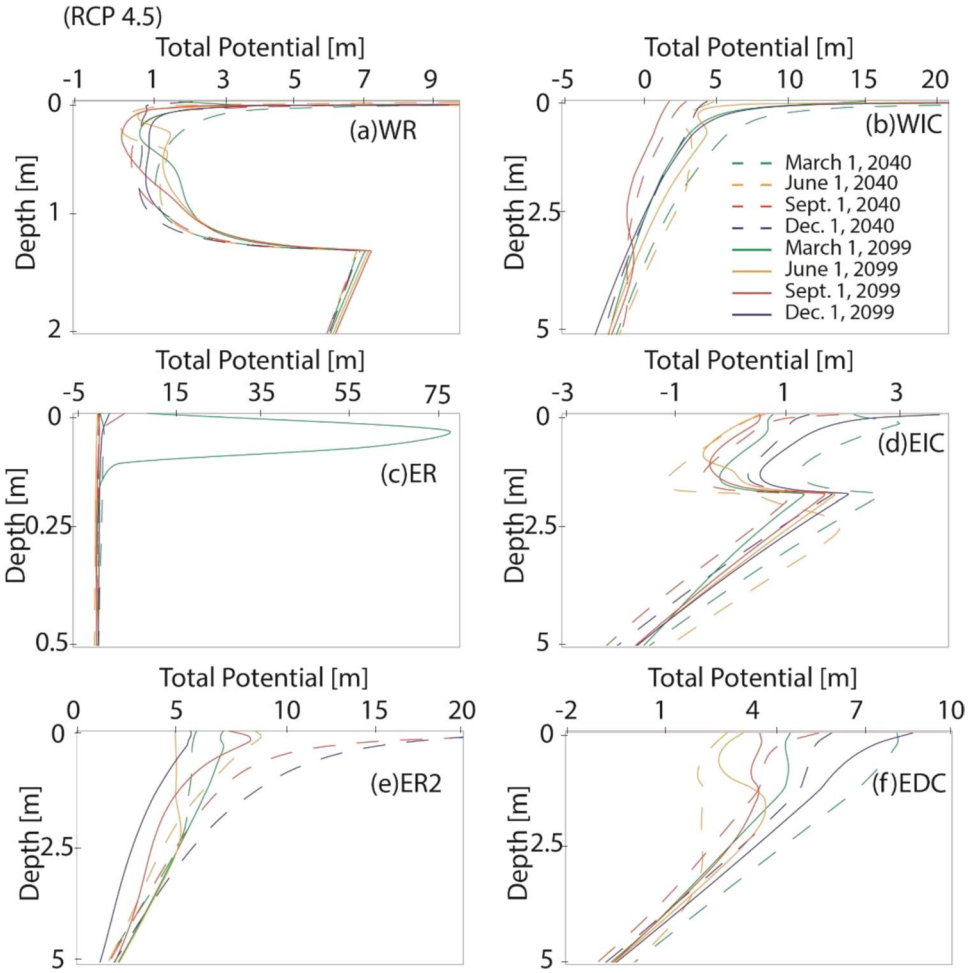

Fig. 10 Simulated future total potential profiles of CANESM2 GCM at RCP 4.5 calculated from Hydrus-1D head at depth output at sites **a** western rangeland (WR), **b** western irrigated corn (WIC), **c** eastern rangeland (ER), **d** eastern irrigated corn (EIC), **e** eastern rangeland 2 (ER2), and **f** eastern dryland corn (EDC). Dashed lines represent months in the year 2040 and solid lines represent months in the year 2099. The top several meters are shown to highlight the variability in this part of the vadose zone

Historic total potential profiles

Total potential profiles were simulated using the Hydrus-1D models for each of the six sites with recent historical atmospheric and meteorological inputs from the years 2008–2018 (Fig. 9). The simulated head at vertical depths within the vadose zone for the first of every March, June, September, and December during the most recent dry and wet periods were used to calculate total potential profiles. The dates shown in Fig. 9 were selected because they encompass the peak dry and wet PDSI values during the most recent dry and wet periods (Table 4).

Most of the variability in the total potential profile occurs in the top few meters of the vadose zone (Fig. 9). The deeper total potential profiles that are not shown in Fig. 9 all generally have a downward and 1:1-unit gradient profile that indicates gravity-dominated flow, which is similar to the total potential profiles shown in Fig. 1a beneath approximately 3 m below land surface. Both western sites (WR and WIC) showed downward flux occurring shallower in the profile during the dry period compared to the wet period. In general, the eastern sites (ER, ER2, EIC, and EDC) showed more downward flux in the 2012 dry period but with seasonal upward flux in the top meter for sites ER2, EIC, and EDC. This indicates that in times of drought, total potential in the eastern sites, with greater average annual precipitation than the western sites, are more sensitive to seasonal fluctuations and have periods of upward water flux in the near-surface vadose zone.

As mentioned earlier, the difference in the simulated recharge rates beneath ER and ER2 is explained by their contrasting total potential profiles (Fig. 9c and e). Site ER has a nearly vertical total potential slope, indicating little to no flux, except in the top 0.1 m of the vadose zone. The relatively lower total potential values are the result of relatively drier water contents and less water storage in the vadose zone, which is a function of relatively lower residual and saturated water content in the vadose zone at site ER (Table S1 of the ESM). Whereas, site ER2 has much greater total potential values and wider fluctuations reaching deeper in the vadose zone and a more positive total potential slope, meaning large water content and relatively more downward flux compared to site ER. The greater total potential values and wider fluctuations at deeper depths is a function of the

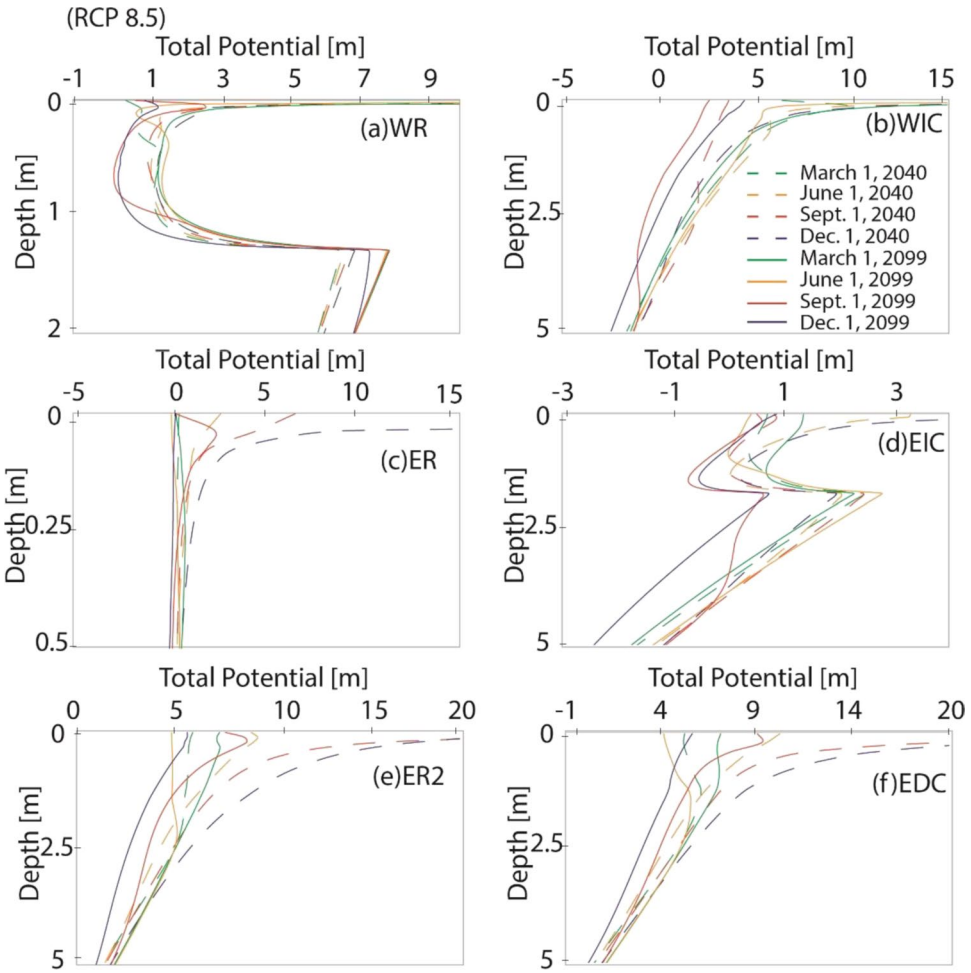

Fig. 11 Simulated future total potential profiles of CANESM2 GCM at RCP 8.5 calculated from Hydrus-1D head at depth output at sites **a** western rangeland (WR), **b** western irrigated corn (WIC), **c** eastern rangeland (ER), **d** eastern irrigated corn (EIC), **e** eastern rangeland 2 (ER2), and **f** eastern dryland corn (EDC). Dashed lines represent months in the year 2040 and solid lines represent months in the year 2099. The top several meters are shown to highlight the variability in this zone of the vadose zone

Table 3 Lag correlations of simulated historic recharge time series calculated in Hydrus-1D and PDSI value time series

Site	Phase lag (months)	Correlation coefficient
WIC	24	0.413
ER	108	0.342
ER2	58	0.543
EIC	22	0.566
EDC	20	0.567

relatively greater residual and saturated water content in the vadose zone at site ER2 as compared to site ER (Table S1 of the ESM). Given the similar atmospheric forcing and land use at ER and ER2, the difference in the total potential profile dynamics and resulting recharge fluxes between the sites illustrates the importance of vadose zone hydraulic properties as a control on recharge.

The west–east variability in hydroclimate appears to be a controlling factor on the total potential profile responses to periods of drought and increased precipitation (Fig. 9). The western sites (WR and WIC) total potential profiles respond as expected with less downward water flux in periods of drought and more downward flux in periods of increased precipitation. The eastern sites, which receive more annual precipitation than the western sites, exhibit the opposite response with less downward water flux in periods of increased precipitation and seasonal upward water flux in times of drought, which may be attributed to the spatial differences in ET during high precipitation periods.

Future total potential profiles

Simulated future total potential profiles were constructed for each of the six sites using the CANESM2 GCM under RCP 4.5 (Fig. 10) and RCP 8.5 (Fig. 11). Hydrus-1D simulated head at depth were used to calculate total potential profiles for the first of every March, June, September, and December for the years 2040 and 2099 and are displayed in Figs. 10 and 11. In both figures, only the top few meters of the vadose zone are depicted because each site has uniform total potential slopes below what is shown, as explained previously for the historical total potential profile results.

Under RCP 4.5 (Fig. 10), there is little variation in total potential profiles between 2040 and 2099 at any site.

Table 4 Historic wet and dry periods chosen for comparison based on PDSI values with modeled historic median recharge of each period

	Time period (month/year)	Duration (months)	PDSI min.	PDSI max.	PDSI median	Median recharge (mm/month)					
						WR	WIC	ER2	ER	EIC	EDC
Wet periods	1/1950–5/1952	29	0.67	7.13	3.10	0.15	6.03	14.3	2.28	20.0	14.4
	5/1982–1/1988	69	1.15	6.19	3.34	0.22	9.97	17.9	1.99	30.7	12.6
	7/1992–8/1999	86	0.89	8.23	3.44	0.23	13.0	15.9	2.97	28.0	14.1
	12/2006–8/2011	57	1.28	7.40	4.64	0.29	19.1	20.7	2.54	29.8	8.93
	6/2014–12/2018	51	0.57	5.36	2.31	0.33	8.85	9.20	1.98	19.3	16.3
Dry periods	8/1953–3/1957	44	-7.11	-1.06	-4.20	0.15	5.74	8.90	2.23	17.1	16.2
	7/1974–2/1977	32	-3.17	-0.67	-1.62	0.21	7.84	13.0	1.48	25.4	11.1
	6/1988–9/1991	40	-4.50	-0.71	-3.20	0.23	16.7	10.6	2.43	21.0	19.1
	3/2002–8/2004	30	-4.87	-1.17	-3.05	0.24	8.75	8.31	3.02	16.7	16.9
	3/2012–5/2014	27	-6.34	-1.10	-3.29	0.31	11.3	14.9	2.00	26.6	22.0

Strong seasonal variations can be seen in the corn crop sites (WIC, EIC, and EDC) with less wetting (increasing total potential values) in the months of June and September compared to the months of December and March. The rangeland sites (WR, ER, and ER2) did not show as much seasonal variation. It is important to note that the abrupt changes in the total potential profiles of sites WR and EIC at respective depths of 1.3 and 1.7 m (Figs. 10 and 11) are associated with changes in the soil layers and associated hydraulic parameters. These abrupt changes in total potential profiles are caused because both profiles at those depths have sediment with relatively lower saturated hydraulic conductivity overlying sediment with relatively higher saturated hydraulic conductivity (Table S1 of the ESM). Instances of simulated seasonal upward water flux occur at each site with the exception of site ER. Under RCP 8.5 (Fig. 11), more variation is displayed in total potential profiles from 2040 and 2099 at each site, especially for the months of September and December, which are periods with the lowest downward water flux. Under RCP 8.5, each site has seasonal upward flux in the year 2099.

A major finding is that upward flux is simulated at all sites by the end of the 21st century under RCP 8.5. Future projections of total potential profiles seem to be more directly controlled by LULC than location (west and east) as was the case with historic total potential profiles. Seasonal variation in future projected total potential gradients is considerable at the corn crop sites under RCP 4.5 in 2099, but upward flux is simulated at every site in 2099 under RCP 8.5. These model results indicate more seasonal upward water flux, regardless of LULC, in the future, particularly under the RCP 8.5 scenario. The greater occurrence of the seasonal upward total potential profiles is the limiting process that explains the statistically lower future projected recharge by the end of the 21st century (Fig. 6).

Conclusions

This study concludes that total potential profiles are likely to be fundamentally altered because of future climate change over the 21st century. To better understand how recharge may respond to climate variability and change in semiarid to arid locations with thick vadose zones, Hydrus-1D was used to simulate historic and future recharge and total potential profiles of six representative study sites in the northern High Plains aquifer. Historical and future recharge and total potential profiles were analyzed to assess controlling factors of recharge: LULC, climate conditions (precipitation, air temperature), and recharge mechanisms (diffuse and irrigation recharge).

Historic precipitation data shows a strong west–east gradient with higher precipitation in the east. Nine LOCA downscaled GCMs each at an RCP of 4.5 and 8.5 show projected increases in future precipitation for each of the six study sites with larger increases under RCP 8.5. The Penman-Monteith calculations from the GCMs inputs in Hydrus-1D indicate higher ET in the west than in the east and show projected increases in future ET for each of the six study sites with larger increases under RCP 8.5. CROPSIM calculated irrigation requirements for all the GCM Hydrus simulations for sites WIC and EIC indicate larger requirements in the west and are projected to increase over time at both sites under RCP 8.5.

Future projections of recharge simulated by the GCM input to Hydrus-1D models indicate more recharge in the east than in the west with respect to LULC; this is consistent with the west/east precipitation gradient of the area. More recharge is projected under irrigated sites than their respective rangeland sites (west and east). Recharge is projected to decrease at each site over the 21st century under RCP 8.5 climate change scenario. In the east, recharge under dryland corn (EDC) falls between ER and EIC. ER2 shows more recharge than ER but their total potential profiles show that

downward flux reaches deeper in the vadose zone under ER2 than ER, which has a nearly vertical total potential slope indicating very little flux in the vadose zone. These results indicate that climate conditions, particularly with the climate change RCP 8.5 scenario, and LULC are large controlling factors on recharge.

Historic recharge time series of each site, except WR, are phase lag correlated to PDSI value time series. Faster responses in recharge to drought and wet periods indicated by PDSI values were identified at all three corn crop sites (WIC, EIC, and EDC) with lag times ranging from 20 to 24 months. All rangeland sites (WR, ER, and ER2) had much slower responses to drought and wet periods indicated by PDSI values with lag times ranging from 58 to 372 months. These findings indicate that LULC is an important filter that can attenuate or amplify the responses in recharge to climate variability.

Historic total potential profiles of the most recent wet and dry period show western sites (WR and WIC), which receive lower annual average precipitation than eastern sites, have less downward water flux during dry periods compared to wet periods. The opposite finding occurs at the eastern sites (ER, ER2, EIC, and EDC)—wet periods show less downward water flux compared to dry periods. However, the eastern sites have seasonal upward flux during the dry period. These findings indicate that the total potential profiles at all sites respond to wet and dry periods but differ in their responses based on the gradient in annual average precipitation inherent within this study site.

An important conclusion of this study is that total potential profiles that control recharge rates may fundamentally change, including a greater occurrence of seasonal upward total potential gradients under future projected climate change across a range of LULC settings. Future total potential profiles for the years 2040 and 2099 have similar patterns to that of the historic total potential profiles. Seasonal variation is considerable at the corn crop sites under RCP 4.5 in 2099 but upward water flux is simulated at every site in 2099 under RCP 8.5. These findings indicate more occurrence of seasonal upward total potential gradients that drives upward water flux, regardless of LULC, near the end of the 21st century under the RCP 8.5. These changes in the total potential gradient would effectively limit the downward flux of water in the vadose zone and subsequent recharge rates. Such changes to the total potential profiles and recharge processes may further challenge the long-term sustainability of some groundwater systems that support irrigated agriculture in semiarid or arid climates. Findings from this study provide a better understanding of the factors that affect recharge rates and mechanisms in thick vadose zones of semiarid and arid climates, and these findings can be used to better constrain future groundwater budgets and inform groundwater sustainability planning and related policy decisions.

Supplementary Information The online version contains supplementary material available at https://doi.org/10.1007/s10040-022-02504-6.

Acknowledgements We thank Duane Woodward (CPNRD, retired), Chris Hobza (USGS), and Greg Steele (USGS, retired) for helping with the installation, maintenance, and data sharing from the vadose zone monitoring network. We also acknowledge the World Climate Research Programme's Working Group on Coupled Modelling, which is responsible for CMIP, and thank the climate modeling groups (listed in Table 2) for producing and making available their model output. For CMIP, the US Department of Energy's Program for Climate Model Diagnosis and Intercomparison provides coordinating support and led the development of software infrastructure in partnership with the Global Organization for Earth System Science Portals.

Funding This research was funded by a grant from the Water Sustainability Fund of the Nebraska Natural Resources Commission in collaboration with the Central Platte Natural Resources District (CPNRD), US Geological Survey (USGS) Nebraska Water Science Center, and San Francisco State University. This research was also supported by a David and Doris Dawdy Hydrologic Sciences Research Grant.

Declarations

Conflict of interest On behalf of all authors, the corresponding author states that there is no conflict of interest.

References

Ajami H, McCabe MF, Evans JP, Stisen S (2014) Assessing the impact of model spin-up on surface water-groundwater interactions using an integrated hydrologic model. Water Resour Res 50:2636–2656. https://doi.org/10.1002/2013WR014258

Anderson MP, Woessner WW, Hunt RJ (2015) Applied groundwater modeling: simulation of flow and advective transport. Elsevier, Amsterdam, 564 pp

Bracken C (2016) Downscaled CMIP3 and CMIP5 climate projections-addendum, release of downscaled CMIP5 climate projections (LOCA) and comparison with preceding information. US Dept. Int. Bureau of Reclamation, Washington, DC, 29 pp

Campbell Scientific Inc. (2009) 229 heat dissipation matric water potential sensor instruction manual. Campbell, Logan, UT, 28 pp. http://s.campbellsci.com/documents/cr/manuals/229.pdf. Accessed 30 May 2022

Carvalho Resende T, Longuevergne L, Gurdak JJ, Leblanc M, Favreau G, Ansems N, Van der Gun J, Gaye CB, Aureli A (2018) Assessment of climate variability impacts on groundwater resources for improved water management and policy in Africa. Hydrogeol J. https://doi.org/10.1007/s10040-018-1864-5

Clarke L, Edmonds J, Pitcher H, Reilly J, Richels R (2007)Scenarios of greenhouse gas emissions and atmospheric concentrations. Sub-Report 2.1a of Synthesis and Assessment Product 2.1 by the US Climate Change Science Program and the Subcommittee on Global Change Research, Department of Energy, Office of Biological & Environmental Research, Washington, DC. https://digitalcommons.unl.edu/cgi/viewcontent.cgi?article=1011&context=usdoepub. Accessed 30 May 2022

Corona CR, Gurdak JJ, Dickinson JE, Ferre TPA, Maurer E (2018) Climate variability and vadose zone controls on damping of transient recharge. J Hydrol 561:1094–1104. https://doi.org/10.1016/j.jhydrol.2017.08.028

Crosbie RS, Dawes WR, Charles SP, Mpelasoka FS, Aryal S, Barron O, Summerell GK (2011) Differences in future recharge estimates due to GCMs, downscaling methods and hydrological models. Geophys Res Lett 38. https://doi.org/10.1029/2011GL047657

Crosbie RS, Scanlon BR, Mpelasoka FS, Reedy RC, Gates JB, Zhang L (2013) Potential climate change effects on groundwater recharge in the High Plains Aquifer, USA: climate change effects on recharge in the High Plains. Water Resour Res 49:3936–3951. https://doi.org/10.1002/wrcr.20292

Dickinson JE, Hanson RT, Predmore SK (2014) HydroClimATe: hydrologic and climatic analysis toolkit. In: Hydrologic analysis and interpretation. Techniques and Methods. US Geological Survey, Reston, VA, 48 pp

Feddes RA, Kowalik PJ, Zaradny H (1978) Simulation of field water use and crop yield. In: Simulation monographs. Wiley, Chichester, UK

Green TR, Taniguchi M, Kooi H, Gurdak JJ, Allen DM, Hiscock KM, Treidel H, Aureli A (2011) Beneath the surface of global change: impacts of climate change on groundwater. J Hydrol 405:532–560. https://doi.org/10.1016/j.jhydrol.2011.05.002

Gurdak JJ (2017) Groundwater: climate-induced pumping. Nat Geosci 10:71–72. https://doi.org/10.1038/ngeo2885

Gurdak JJ, Hanson RT, McMahon PB, Bruce BW, McCray JE, Thyne GD, Reedy RC (2007) Climate variability controls on unsaturated water and chemical movement, High Plains aquifer, USA. Vadose Zone J 6:533. https://doi.org/10.2136/vzj2006.0087

Gurdak JJ, McMahon PB, Dennehy KF, Qi SL (2009) Water quality in the High Plains aquifer, Colorado, Kansas, Nebraska, New Mexico, Oklahoma, South Dakota, Texas, and Wyoming, 1999-2004. US Geol Surv Circ 63

Healy RW (2010) Estimating groundwater recharge. Cambridge University Press, New York, 245 pp

Helsel DR, Hirsch RM (1992) Statistical methods in water resources. Elsevier, Amsterdam

Holman IP, Allen DM, Cuthbert MO, Goderniaux P (2011) Towards best practice for assessing the impacts of climate change on groundwater. Hydrogeol J 20:1–4. https://doi.org/10.1007/s10040-011-0805-3

JMP (2010) Using JMP, version 9. JMP, Cary, NC, 540 pp

Konikow LF (2013) Groundwater depletion in the United States (1900—2008). US Geol Surv Sci Invest Rep 2013-5079, 63 pp. https://doi.org/10.3133/sir20135079

Konikow LF (2015) Long-term groundwater depletion in the United States. Groundwater 53:2–9. https://doi.org/10.1111/gwat.12306

Kuss AJM, Gurdak JJ (2014) Groundwater level response in U.S. principal aquifers to ENSO, NAO, PDO, and AMO. J Hydrol 519:1939–1952. https://doi.org/10.1016/j.jhydrol.2014.09.069

Lauffenburger ZH, Gurdak JJ, Hobza C, Woodward D, Wolf C (2018) Irrigated agriculture and future climate change effects on groundwater recharge, northern High Plains aquifer, USA. Agric Water Manag 204:69–80. https://doi.org/10.1016/j.agwat.2018.03.022

Li H, Sheffield J, Wood EF (2010) Bias correction of monthly precipitation and temperature fields from Intergovernmental Panel on Climate Change AR4 models using equidistant quantile matching. J Geophys Res 115:D10101. https://doi.org/10.1029/2009JD012882

Maurer EP, Brekke L, Pruitt T, Thrasher B, Long J, Duffy P, Dettinger M, Cayan D, Arnold J (2014) An enhanced archive facilitating climate impacts and adaptation analysis. Bull Am Meteorol Soc. https://doi.org/10.1175/bams-d-13-00126.1

McMahon PB, Dennehy KF, Michel RL, Sophocleous MA, Ellett KM, Hurlbut DB (2003) Water movement through thick unsaturated zones overlying the central High Plains aquifer, southwestern Kansas, 2000–2001. US Geological Survey, Reston, VA, 39 pp

McMahon PB, Dennehy KF, Bruce BW, Böhlke JK, Michel RL, Gurdak JJ, Hurlbut DB (2006) Storage and transit time of chemicals in thick unsaturated zones under rangeland and irrigated cropland, High Plains, United States. Water Resour Res 42. https://doi.org/10.1029/2005WR004417

McMahon PB, Dennehy KF, Bruce BW, Gurdak JJ, Qi SL (2007) Water-quality assessment of the High Plains Aquifer, 1999–2004. US Geol Surv Prof Pap 1749, 136 pp

McMahon PB, Plummer LN, Böhlke JK, Shapiro SD, Hinkle SR (2011) A comparison of recharge rates in aquifers of the United States based on groundwater-age data. Hydrogeol J 19:779–800

Meixner T, Manning AH, Stonestrom DA, Allen DM, Ajami H, Blasch KW, Brookfield AE, Castro CL, Clark JF, Gochis DJ, Flint AL, Neff KL, Niraula R, Rodell M, Scanlon BR, Singha K, Walvoord MA (2016) Implications of projected climate change for groundwater recharge in the western United States. J Hydrol 534:124–138. https://doi.org/10.1016/j.jhydrol.2015.12.027

Moeck C, Grech-Cumbo N, Podgorski J, Bretzler A, Gurdak JJ, Berg M, Schirmer M (2020) A global-scale dataset of direct natural groundwater recharge rates: a review of variables, processes and relationships. Sci Total Environ 717. https://doi.org/10.1016/j.scitotenv.2020.137042

NOAA (2018) National Climatic Data Center. https://www.ncdc.noaa.gov/. Accessed 30 May 2022

NOAA (2021) National Centers for Environmental Information, Climate at a Glance, Divisional Time Series, Palmer Drought Severity Index (PDSI). https://www.ncei.noaa.gov/. Accessed 30 May 2022

Pierce DW, Cayan DR, Thrasher BL (2014) Statistical downscaling using localized constructed analogs (LOCA). J Hydrometeorol 15:2558–2585. https://doi.org/10.1175/JHM-D-14-0082.1

Pierce DW, Cayan DR, Maurer EP, Abatzoglou JT, Hegewisch KC (2015) Improved bias correction techniques for hydrological simulations of climate change. J Hydrometeorol 16:2421–2442. https://doi.org/10.1175/JHM-D-14-0236.1

Polade SD, Gershunov A, Cayan DR, Dettinger MD, Pierce DW (2013) Natural climate variability and teleconnections to precipitation over the Pacific-North American region in CMIP3 and CMIP5 models: climate variability in CMIP5 models. Geophys Res Lett 40:2296–2301. https://doi.org/10.1002/grl.50491

Radcliffe DE, Šimůnek J (2010) Soil Physics with HYDRUS: modeling and applications. CRC, Boca Raton, FL, 373 pp

RCP Database (version 2.0) (2009) RCP database. https://tntcat.iiasa.ac.at/RcpDb/dsd?Action=htmlpage&page=welcome. Accessed 30 May 2022

Re V, Maldaner C, Gurdak JJ, Leblanc M, Carvalho Resende T, Stigter TY (2018) Topical Collection: Climate change research by early-career hydrogeologists. Hydrogeol J. https://doi.org/10.1007/s10040-018-1730-5

Riahi K, Grueble A, Nakicenovic N (2007) Scenarios of long-term socio-economic and environmental development under climate stabilization. Technol Forecast Soc Change 74:887–935

Richards L (1931) Capillary conduction of liquids in porous mediums. Physics 1:318–333

Scanlon BR, Keese K, Reedy RC, Simunek J, Andraski BJ (2003) Variations in flow and transport in thick desert vadose zones in response to paleoclimatic forcing (0–90 kyr): field measurements, modeling, and uncertainties—flow in the vadose zones in response to paleoclimatic forcing. Water Resour Res 39. https://doi.org/10.1029/2002WR001604

Scanlon BR, Reedy RC, Stonestrom DA, Prudic DE, Dennehy KF (2005) Impact of land use and land cover change on groundwater recharge and quality in the southwestern US. Glob Chang Biol 11:1577–1593. https://doi.org/10.1111/j.1365-2486.2005.01026.x

Schaap MG, Leij FJ, van Genuchten MT (2001) ROSETTA: a computer program for estimating soil hydraulic parameters with hierarchical pedotransfer functions. J Hydrol 251:163–176

Seck A, Welty C, Maxwell RM (2015) Spin-up behavior and effects of initial conditions for an integrated hydrologic model: spin-up behavior and effects of initial conditions. Water Resour Res 51:2188–2210. https://doi.org/10.1002/2014WR016371

Šimůnek J, van Genuchten MT, Šejna M (2008) Development and applications of the HYDRUS and STANMOD software packages and related codes. Vadose Zone J 7:587–600. https://doi.org/10.2136/vzj2007.0077

Šimůnek J, Sejna M, Saito H, Sakai M, van Genuchten MT (2013) The HYDRUS-1D software package for simulating the one-dimensional movement of water, heat, and multiple solutes in variably-saturated media. Department of Environmental Sciences, University of California Riverside, Riverside, CA

Smidt SJ, Haacker EMK, Kendall AD, Deines JM, Pei L, Cotterman KA, Li H, Liu X, Basso B, Hyndman DW (2016) Complex water management in modern agriculture: trends in the water-energy-food nexus over the High Plains Aquifer. Sci Total Environ 566–567:988–1001. https://doi.org/10.1016/j.scitotenv.2016.05.127

Smith SJ, Wigley TML (2006) Multi-gas forcing stabilization with minicam. Energy J. SI2006. https://doi.org/10.5547/ISSN0195-6574-EJ-VolSI2006-NoSI3-19

Steele GV, Gurdak JJ, Hobza CM (2014) Water movement through the unsaturated zone of the High Plains Aquifer in the Central Platte Natural Resources District, Nebraska, 2008–12. US Geol Surv Sci Invest Rep 2014-5008

Stocker T (ed) (2014) Climate change 2013: the physical science basis: Working Group I contribution to the Fifth assessment report of the Intergovernmental Panel on Climate Change. Cambridge University Press, New York

Szilagyi J, Zlotnik VA, Gates JB, Jozsa J (2011) Mapping mean annual groundwater recharge in the Nebraska Sand Hills, USA. Hydrogeol J 19:1503–1513. https://doi.org/10.1007/s10040-011-0769-3

Szilagyi J, Zlotnik VA, Jozsa J (2013) Net recharge vs. depth to groundwater relationship in the Platte River valley of Nebraska, United States. Groundwater 51:945–951. https://doi.org/10.1111/gwat.12007

Taylor RG, Scanlon B, Döll P, Rodell M, van Beek R, Wada Y, Longuevergne L, Leblanc M, Famiglietti JS, Edmunds M, Konikow L, Green TR, Chen J, Taniguchi M, Bierkens MFP, MacDonald A, Fan Y, Maxwell RM, Yechieli Y et al (2012a) Ground water and climate change. Nat Clim Chang 3:322–329. https://doi.org/10.1038/nclimate1744

Taylor KE, Stouffer RJ, Meehl GA (2012b) An overview of CMIP5 and the experiment design. Bull Am Meteorol Soc 93:485–498. https://doi.org/10.1175/BAMS-D-11-00094.1

Thornton PE, Running SW, White MA (1997) Generating surfaces of daily meteorological variables over large regions of complex terrain. J Hydrol 190:214–251. http://www.daymet.org/default.jsp. Accessed 20 Jan 2007

Treidel H, Martin-Bordes JL, Gurdak JJ (eds) (2012) Climate change effects on groundwater resources: a global synthesis of findings and recommendations, 1st edn. Balkema, Leiden, The Netherlands

USGS (2022) National Water Information System (NWIS), U.S. Geological Survey. http://waterdata.usgs.gov/nwis. Accessed 30 May 2022

Velasco EM, Gurdak JJ, Dickinson JE, Ferre TPA, Corona C (2017) Interannual to multidecadal climate forcings on groundwater resources of the west coast of the US. J Hydrol: Regional Stud 11:250–265. https://doi.org/10.1016/j.ejrh.2015.11.018

Walvoord MA, Stonestrom DA, Andraski BJ, Striegl RG (2004) Constraining the inferred paleohydrologic evolution of a deep unsaturated zone in the Amargosa Desert. Vadose Zone J 3:502–512. https://doi.org/10.2136/vzj2004.0502

Wellings SR, Bell JP (1982) Physical controls of water movement in the unsaturated zone. Q J Eng Geol Lond 15:235–241

Wesseling JG, Elbers JA, Kabat P, Van den Broek BJ (1991) SWATRE: Instructions for input. Work Group SWAP. https://core.ac.uk/download/pdf/29344298.pdf. Accessed June 2022

Wise M, Calvin K, Thomson A, Clarke L, Bond-Lamberty B, Sands R, Smith S, Janetos A, Edmonds J (2009) Implications of limiting CO2 concentrations for land use and energy. Science 324(5931):1183–1186